

Article ID: 1000-5641(2015)03-0105-11

Characterization of and insight into the electrochemistry of MoS_2

ZHANG Xian-hui, CHEN Zhen-lian,
CHEN Xiao-bo, LI Jun

(Ningbo Institute of Materials Technology and Engineering, Chinese Academy of Sciences,
Ningbo Zhejiang 315201, China)

Abstract: By combining experimental methods with first-principles calculations this article reports the determination of the structural characters of MoS_2 in the first discharging and charging cycling, where the first stage phase transformation occurs. The significant voltage plateau at 1.1 V is attributed to lithium insertion on octahedral vacancy sites of $2\text{H-Li}_x\text{MoS}_2$ with lithium concentration (x) up to 0.56, which corresponds with the calculated voltage and phase stability of MoS_2 . However, the ensuing amorphization for x over 1.0 immediately removes the plateau character from the charging curve. Furthermore, we offer a comparison to LiCoO_2 to investigate the physical mechanism of the anode and cathode voltaic.

Key words: lithium-ion batteries; MoS_2 ; structural characters; electrochemistry; first-principles calculations

CLC number: O646.21 **Document code:** A

DOI: 10.3969/j.issn.1000-5641.2015.03.013

MoS_2 的电化学表征与探究

张贤惠, 陈珍莲, 陈晓波, 黎 军

(中国科学院 宁波材料技术与工程研究所, 浙江 宁波 315201)

摘要: 结合实验和第一性原理计算, 对 MoS_2 首次充放电过程中的第一阶段相变的结构变化进行了研究. 研究表明1.1 V处的电压平台对应于锂离子嵌入量0.56, 锂离子都是嵌入2H相的八面体空位, 与计算出的平台电压值及 MoS_2 的相稳定特性都相吻合. 但当锂离子嵌入量超过1.0时, 晶体结构向无定形结构转变, 导致后续充电过程中不出现平台特征. 此外, 通过对比 MoS_2 和 LiCoO_2 的嵌入能量项, 本文探究了决定正极与负极材料本征电压差的物理机制.

关键词: 锂离子电池; MoS_2 结构特性; 电化学性能; 第一性原理计算

收稿日期: 2014-03

基金项目: 国家自然科学基金(11174301, 21303235); 973计划(2012CB722700); 863计划(2013AA050901); 宁波市创新团队(2011B82005)

第一作者: 张贤惠, 女, 硕士研究生, 研究方向为锂离子电池. E-mail: zhangxianhui@nimte.ac.cn.

通信作者: 陈珍莲, 女, 助理研究员, 研究方向为材料物理与化学. E-mail: chenlz@nimte.ac.cn.

0 Introduction

The prevalence of lithium ion battery (LIB) technology creates a strong demand of advanced electrode materials. A significant part of this need is to identify suitable van der Waals-bonded layered materials as the anode for lithium ion batteries. Graphitic carbon is the most commonly used layered materials for the anode due to their low cost, flat voltage profile, and good structural stability during cycling^[1-4]. Nevertheless, graphitic materials suffer from a relatively low specific capacity of $372 \text{ mAh}\cdot\text{g}^{-1}$ and the easy formation of lithium dendrite at high rate^[5]. Among the non-carbon layered materials explored for the anode of lithium ion batteries, transition metal dichalcogenides, especially MoS_2 , provide a potentially impactful alternative to graphite.

As a typical layered transition metal sulfide, MoS_2 occupies a high competitive position as a promising anode material for Li-ion battery due to the high reversible capacity and excellent rate capability^[6]. Similar to graphite, MoS_2 has a pronounced hexagonal layered lattice^[7], in which three-atom (S-Mo-S) slabs stack together by weak van der Waals interactions and this particular structure allows Li^+ to intercalate into and exfoliate from the vacant space between slabs easily^[8,9]. During the charging and discharging, interestingly, the lithiation mechanisms of MoS_2 vary with the cut-off voltage at discharge. When the cut-off voltage is around 1.1 V *vs.* Li/Li^+ , the lithium intercalation is generally considered as an ion and electron transfer topotactic reaction^[10-12]; when below 1.1 V, one or a series of decomposition reactions arise^[13-15]. Elemental sulfur has been even proposed to be responsible for the special electrochemical activity just after the initial lithiation^[16]. However, the definitive structural forms with different imbedded lithium concentration are still not fully understood for different cut-off voltages. Also, the physical origin of the observed high specific capacities of MoS_2 over just one lithium insertion in the ranges of 0.01~3.0 V has not been explained very well.

Due to the unique chemical and physical properties, MoS_2 has attracted intensive studies via experimental and computational methods over the past years, mainly focusing on two themes. The first one focuses on developing materials synthesis, especially, in nanostructures to improve electrochemical performance as the anode for lithium ion batteries^[17-21]. The other one primarily concerns on the structural transformation upon lithium insertion or extraction^[22-26]. However, few studies have devoted to understand the key structure character that determines the electrochemical properties of MoS_2 for the potential application to the anode of lithium ion batteries.

The key aspect of this work is to offer a systematical study to understand the structural evolution of MoS_2 upon Li intercalation by an integrated approach of experiments and first-principles calculations. Firstly, we present a variety of experimental characterizations of the material used in this study. Then, we focus on the details of the structural character in the first discharging and charging cycling by invoking first-principles determination of the voltage and phase stability. Furthermore, we offer a theoretical examination of the intrinsic voltaic

difference between the anode and cathode from the physical mechanism of lithium intercalation. We believe that such a fundamental understanding may provide insights into the nature of intercalation compounds beyond the apparent difference in voltage values and may finally benefit the development of electrode materials in general.

1 Experimental methods

1.1 Sample analysis

Commercial MoS₂ powder by China Molybdenum Industry was used in this study. The crystal structure was characterized by X-ray diffraction (XRD) with Cu K α ($\lambda=0.154\ 18\ \text{nm}$) radiation (Bruker AXS, D8 Advance). The morphology and microstructure were observed with Field Emission Scanning Electron Microscope (FESEM, Hitachi, S-4800). The particle size distribution was tested with Microtrac Particle Size Analyzer (S3500-special, Microtrac, USA). Brunauer Emmett Teller (BET) surface area was measured with a Micromeritics Instruments ASAP 2020M.

1.2 Electrochemical measurements

For the electrochemical test, MoS₂ powder was used as the active material. The working electrodes were fabricated by mixing 85:5:10 (w/w) ratio of active material, super P carbon and polyvinylidene fluoride (PVDF), respectively, using N-Methyl-pyrrolidone (NMP) as the solvent. The resulting slurry was cast on a Cu or Al current collector, followed by drying at 120 °C for 15 h under vacuum oven. The electrode foils were subsequently pressed and punched into circular disc.

The charge/discharge tests were carried out using CR2032 coin type half-cells comprising of the MoS₂ working electrode, Li metal counter electrode with a 1 mol/L solution of LiPF₆ in ethylene carbonate/dimethyl carbonate (EC/DMC, 1:1, v/v) as the electrolyte, and porous polypropylene separator (Celgard). The cells were assembled in the argon filled glove box where both moisture and oxygen levels are less than 1 mg/m³. Electrochemical performances were evaluated in the voltage ranges of 0.01~3.0 V *vs.* Li/Li⁺ (with copper current collector) and 0.8~3.0 V *vs.* Li/Li⁺ (with aluminum current collector) at 25 °C, with a current density of 100 mA·g⁻¹.

2 Computational methods

All energies, intercalation potentials and geometries of materials in this paper were obtained using first-principles calculation in the generalized gradient approximation (GGA) suggested by Perdew, Burke and Ernzerhof (PBE) [27] within density functional theory (DFT), as implemented in the Vienna Ab initio Simulation Package (VASP)[28,29]. The projector augmented wave (PAW) potential [29,30] were applied to represent the nuclei and core electrons. A simple pair-wise force field proposed by Grimme [31] was adopted describing the van der Waals interactions in totally delithiated phase of MoS₂. The reciprocal space Monkhorst-Pack k-point mesh interval is about 0.04 Å⁻¹. All structures were fully relaxed with respect to internal

and external cell parameters until all forces acting on ions converged to less than 0.01 eV/Å. Detailed structural information of 2H-MoS₂ has been reported in our previous work^[25,26].

The scheme of first-principles calculations of the charged states proposed in ref. [32] is followed to calculate the decomposed intercalation energy terms (the electron affinity E_{ea} , the lithium ion affinity E_{la} , and the structure relaxation energy E_{gr}), the summation of which is the total intercalation energy, directly connected to the first-principles average voltage \bar{V} by Eq. (1),

$$e \cdot \bar{V} = -(E_{\text{ea}} + E_{\text{la}} + E_{\text{er}}). \quad (1)$$

The performance of the calculation is simple and no spurious energy contribution introduced by the jellium charge background^[33,34], different from the charged defect calculation for semiconductor.

3 Results and discussions

3.1 Materials characterization

It is believed that the electrochemical performance of electrode materials is in general significantly influenced by the morphology, microstructure, and particle size of the materials^[35]. Therefore, we performed a systematical characterization of the basic physical chemical properties of MoS₂, including crystal structure, morphology, particle size and the specific surface area before conducting electrochemical evaluation.

SEM images in Figure 1 show that the studied MoS₂ particle is sheet-like with a thickness of ca. 100 nm, corresponding to more than 160 stacked individual S-Mo-S slabs^[22]. Fig. 2 indicates that the particle distributes in a range of 0.5~1.5 μm with a considerably sharp peak almost around 890.8 nm, implying evenly distribution, consistent with the SEM characterization. The specific surface area of the MoS₂ from BET method shows a value of 8.8 m²·g⁻¹, far below that of the nanostructured MoS₂^[14,36,37], consistent with more than 160 stacked slabs.

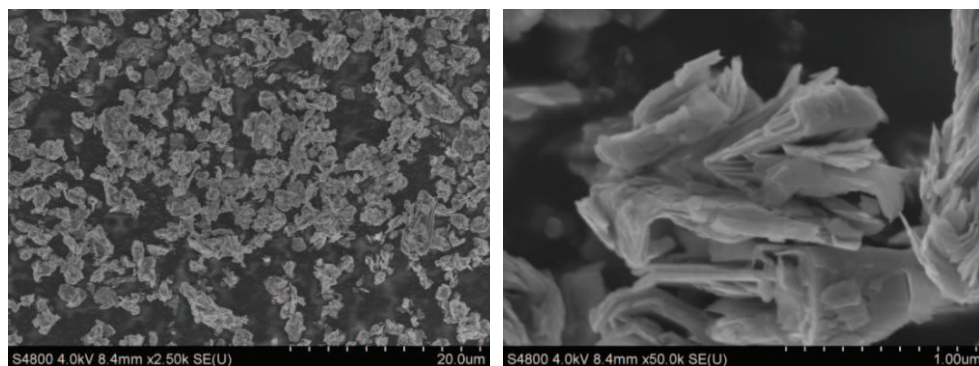


Fig. 1 SEM images of the commercial MoS₂ at different magnifications

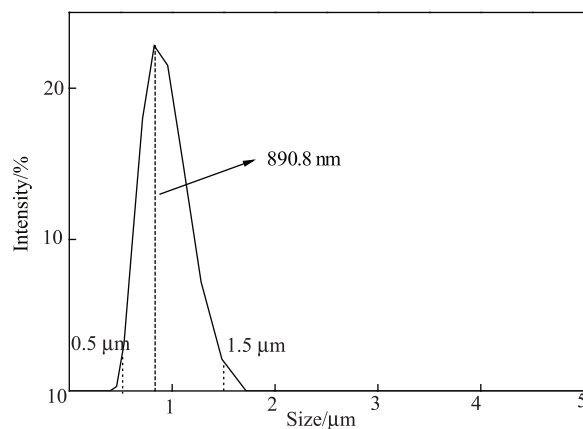
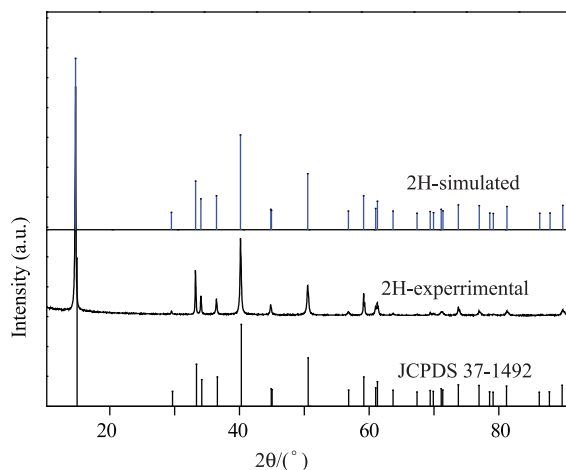


Fig. 2 Size distribution by intensity

The XRD pattern of the pristine MoS₂ is presented with the simulated XRD of first-principles 2H-MoS₂ crystal model in Fig. 3. All the diffraction peaks can be indexed as a 2H structure (JCPDS 37-1492) without any impurity reflections, indicating a pure MoS₂ in 2H phase, agreeing well with the first-principles atomistic model.

Fig. 3 XRD patterns of the studied MoS₂

3.2 Electrochemical Properties

Figure 4 shows the discharging and charging profiles of the sub-micron MoS₂ powder for the first cycle at current density 100 mA·g⁻¹ in the voltage window of 0.01 V to 3.00 V. The first discharging presents two voltage plateaus: 1.1 V (I in Fig. 4) and 0.6 V (II in Fig. 4). The first charging shows a linear segment from 0.01 to 2.11 V (III in Fig. 4). The overall profile agrees with previous reports including nanostructured MoS₂^[13,38,39]. The total discharge capacity is found to be 937 mAh·g⁻¹ with a coulombic efficiency of 65.3%, which should benefit from the sheet-like topography. The linear charging segment up to 2.11 V corresponds to a calculated capacitance of 574 F·g⁻¹, comparable to the capacitance of 550 F·g⁻¹ of graphene with exceptionally high specific surface area up to 2675 m²·g⁻¹^[40]. Both values seem less than

those of nanostructured MoS_2 ^[13,38]. However, the difference appears mainly from the belonging plateau after 0.6 V, instead of the plateau at 1.1 V.

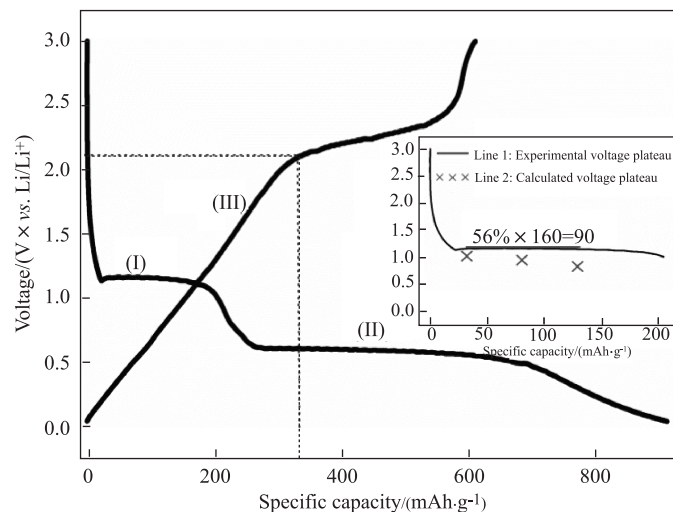


Fig. 4 Initial discharging/charging profiles of the MoS_2 electrodes between 0.01 V and 3.0 V

The MoS_2/Li cell engenders at 1.1 V plateau a specific discharge capacity ca. $200 \text{ mAh}\cdot\text{g}^{-1}$, which is very competitive to the nano-formed MoS_2 previously reported^[13,38]. This is a strong indication of bulk properties, instead of effects of nanostructures. The visible plateau (Line 1, the inset of Fig. 4) agrees well with the calculated average voltage (Line 2, the inset of Fig. 4) and the voltage decaying after more than 56% lithium concentration also agrees well with previous experimental reports^[22,38,39] and correlates with the calculated phase stability^[26].

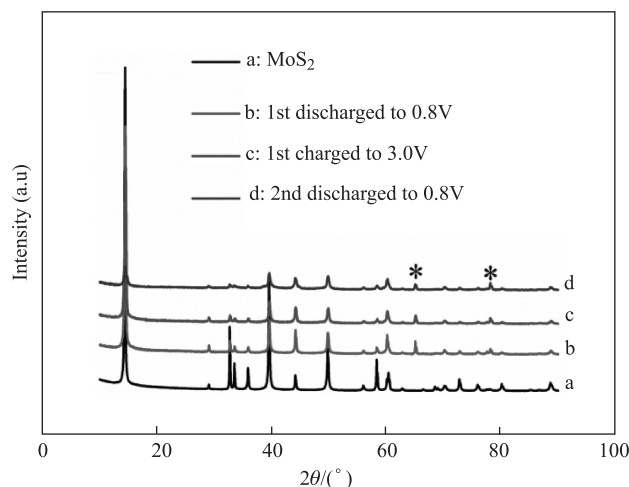
The calculation has found that the total energy of $2\text{H-Li}_x\text{MoS}_2$ is lower than that of $1\text{T-Li}_x\text{MoS}_2$ for concentration less than 56%, after which the 1T phase becomes more stable than the 2H phase^[26]. Therefore, the 1.1 V plateau is attributed to the two-phase lithiation in the 2H host. This is consistent with the discharged capacity of Line 1 presented, $90 \text{ mAh}\cdot\text{g}^{-1}$, an embedded Li content 56% of the theoretical capacity of just one lithiated LiMoS_2 ($160 \text{ mAh}\cdot\text{g}^{-1}$). After 56% concentration, the 2H to 1T phase transition dominates the plateau decaying. Furthermore, the formation energy of one lithium ion on octahedral vacancy site is only 0.623 eV per formula unit lower than that of a pair of lithium ions on tetrahedral vacancy sites in the space between S-Mo-S slabs of the 1T phase^[26]. This corresponds to the voltage difference, $\sim 0.5 \text{ V}$, between the plateau I and II in Figure 4. Therefore, the transition from plateau I to II may attribute to two mechanisms: electron charge-density wave (CDW) formation^[25] and the 2H to 1T lattice transition^[26]. After one lithium ion is fully intercalated into the CDW-1T LiMoS_2 , which is the stable phase according to the calculation^[26], the plateau II develops by shifting intercalated lithium ions from octahedral vacancy sites to tetrahedral vacancy sites of the CDW-1T host, forming lithium ion pairs or clusters at the lower voltage.

The overall capacity, ca. $300\sim 350 \text{ mAh}\cdot\text{g}^{-1}$, of plateau II indicates about two additional lithium ions inserting into the van der Waals gap. However, the van der Waals gap of the $1\text{T-Li}_x\text{MoS}_2$ host cannot offer more than one octahedral and two tetrahedral vacancy sites in a well ordered lattice. Thus, the three-atom (S-Mo-S) slabs are forced to change into an amorphized

structure on high lithium density ($x > 3$). Our calculation of high lithiated structures (over three lithium ions) actually has confirmed the lattice periodicity totally destroyed. This should indicate the amorphization occurs after discharging to 0.01 V. However, so far, the calculation is difficult to confirm whether or not a cluster of elemental sulfur forms, which may be an interesting work in future.

3.3 Structural evolution upon Li intercalation

Since the plateau II involves over lithiation induced amorphization, it is interesting to know the reversibility of the crystal structures for the first plateau at 1.1 V. We perform an ex-situ XRD characterization of the MoS₂ in different cyclings between 0.8 and 3.0 V *vs.* Li/Li⁺ as presented in Figure 5. Because of the close XRD peaks between copper and lithiated MoS₂ at around 44° and 50°^[37], aluminum foil, whose lithiation/delithiation occurs at about 0.4 V *vs.* Li/Li⁺, is employed as the current collector.



Note: (a) pristine material; (b) initially discharged to 0.8 V; (c) firstly charged to 3.0 V; (d) then continuously discharged to 0.8 V. Peaks marked by * correspond to Al current collector

Fig. 5 Ex-situ XRD patterns of the MoS₂

Fig. 5 shows that only the first peak holds in all the ex-situ XRD, indicating the sub-micron thin lamellas remain. The intensity of other primary diffraction peaks fades away continuously, accompanying the vanishing of peaks between 60~70°. It is very remarkable when comparing the XRD patterns of the MoS₂ electrode in the pristine state (Fig. 5a) and even just after firstly discharged to 0.8 V (Fig. 5b). The cycled MoS₂ cannot fully return to its pristine crystalline structure at the end of recharging to 3.0 V as showed in Figure 5c, indicating the irreversibility is associated with the 2H to 1T transition^[25]. These observations imply the building-up of the amorphization of MoS₂ host after the first 2H to 1T transition, resulting from only one lithium insertion and desertion during the cycling between 0.8 V and 3.0 V. However, the 2H to 1T transition has not yielded a fully amorphization.

For the sake of more exact interpretations, various methods have been employed to study the complex mechanisms involved in lithium intercalation into molybdenum disulfide in order to understand the specific forms before and after the structure decomposition^[12,41-43]. Our study

has so far given the detailed structural character that may help interpret the electrochemical properties of MoS_2 during the first discharging and charging cycle. The observed behavior of MoS_2 is a very common electrochemical character of transition metal dichalcogenides, for example, in LiCrS_2 ^[41]. The other layered transition metal dichalcogenides, MS_2 ($M = \text{Ti}, \text{V}, \text{Cr}$), also share the same feature of electrochemical characters within the voltage range of 0.01~2.0 V during the initial discharging and charging processes^[41]. Therefore, they may have similar underlying characters in the structures.

3.4 Electron and ion intercalation

Actually, much less attention has been paid to the nature of voltaic difference between the anode and cathode beyond the obvious voltage values. The voltage of MoS_2 is much lower than cathode materials such as lithium cobalt oxide (LiCoO_2) (2.5~4.5 V *vs.* Li/Li^+). The layer-sliding in graphitic carbons during lithium insertion makes it difficult to make such a direct comparison to lithium cobalt oxide^[36,44]. As we showed in previous section, only a small change in the host lattice below 56% lithium concentration occurs, therefore, MoS_2 may be a good prototype to investigate the intrinsic voltaic difference, which decides the application of intercalation compounds as the anode or the cathode. Here we compare the intercalation energy terms^[32] of MoS_2 and LiCoO_2 by first-principles calculations (showed in Table 1) due to their similar lithium insertion behavior and discuss the physical origin why the plateau voltage of MoS_2 is much lower than that of LiCoO_2 . To further make the comparison rational and complete, the calculations of LiCoS_2 , iso-structured to LiCoO_2 , are also shown in Table 1.

Tab.1 Calculated average voltage \bar{V} (V *vs.* Li/Li^+) and intercalation energy terms (the units are eV per formula unit) of 2H- LiMoS_2 and $R\bar{3}m$ LiCoO_2 , LiCoS_2

	\bar{V}	E_{ea}	E_{la}	E_{gr}
LiMoS₂-GGA	0.79	6.60	-6.99	-0.40
LiCoO₂-GGA	3.46	3.31	-6.32	-0.46
LiCoS₂-GGA	2.06	5.22	-6.87	-0.40

Due to the intrinsic delocalization of the 4*d* electrons and weak crystal field formed by sulfur polyhedron (trigonal prism in 2H- MoS_2), GGA calculation gives values of average voltage relatively close to experiment, while lower value of voltage than experiment for LiCoO_2 is attributed to the intrinsic localization of 3*d* electron and the strong crystal field formed by oxygen polyhedron (octahedron in LiCoO_2). To make the comparison consistent at the same calculation accuracy, GGA calculations are adopted here on account of the almost constant discrepancy between GGA calculations and experiments^[32], and one lithium ion is assumed to intercalate into 2H- MoS_2 before phase transition occurring.

As seen in Tab.1, the difference of intercalation energy between 2H- LiMoS_2 and LiCoO_2 is dominated by the electron intercalation. The value difference is over 3 eV in E_{ea} whereas less than 1 eV in E_{la} and much less in E_{gr} . It is worth to note according to Eq.(1) that the contributions from E_{la} and E_{gr} are to deliver a higher voltage for 2H- LiMoS_2 than LiCoO_2 since the voltage value is larger when the absolute values of E_{la} and E_{gr} are larger. That manifests that the much lower voltage of 2H- LiMoS_2 than that of LiCoO_2 is mainly attributed to the energy cost due to the electron intercalation rather than the ion intercalation.

The energy contribution to the ion intercalation mainly attributes to the Madelung potential for the intercalated Li ion introduced by the electrostatic field. The crystal structure of 2H-LiMoS₂ is quite similar to layered cathode LiCoO₂, with hexagonal S-Mo-S slabs in 2H-LiMoS₂ and O-Co-O in LiCoO₂ stacking along hexagonal *c*-axis. The intercalated Li ion occupies the octahedral site both in 2H-LiMoS₂ and LiCoO₂. That makes the E_{1a} value for 2H-LiMoS₂ close to LiCoO₂ and closer to LiCoS₂.

The energy contributions to the electron intercalation, i.e., the redox energy, are determined by the formal valence state alternation of the active cation and its covalent bonding with the nearest-neighbor anions [40]. Both are related with the degree of the localization of the lowest unoccupied molecular orbital (LUMO) of the host attributing to the intrinsic degree of the localization of the *d*-electron of the transition metal cation and the intensity of the crystal-field. In general, 3*d* electron is intrinsically more localized than 4*d*. Oxygen polyhedron field is stronger than sulfur, thus the *d*-electron in the oxygen polyhedral field is much more localized. Whether centered in trigonal prism or octahedron, the transition metal cation is hex-coordinate and the electrostatic field formed by these two types of polyhedra with the same anions will be very similar. Then, the degree of the localization of the LUMO for the three electrodes in Table 1 can be ranked as LiCoO₂, LiCoS₂ and LiMoS₂. That suggests stronger localization lower energy cost from electron intercalation and thus higher intercalation voltage.

4 Conclusion

In this work, we present a well characterized MoS₂ for its electrochemical application as the anode material for lithium ion battery via an integrated approach of experiment and computation. The studied MoS₂ takes on a considerably uniform distribution around the particle size of 890.8 nm with the specific surface area of 8.8 m²·g⁻¹. In spite of the sub-micron size, it presents an initial discharge capacity of 937 mAh·g⁻¹ in the voltage range of 0.01~3.0 V, which is comparable to some reported nanostructured MoS₂ materials, this may attribute to the bulk properties of sheet liked thin lamellas. And in the cycles between 0.8~3.0 V, we investigate the voltage plateaus and structural evolution with the combination of charging and discharging cycling, XRD patterns and computational models, provide evidences that the lithiated MoS₂ transits from the 2H to 1T form when the inserted Li content reaches more than 56%. Moreover, the physical origin of the low voltaic of MoS₂ is also discussed: it is attributed to the E_{ea} , which represents the energy of electron intercalation into the host, primarily determining the voltaic difference between MoS₂ and LiCoO₂ although they all belong to lithium inserted materials. In summary, a comparatively systematic cognition for the given materials owned a variety of structures, morphologies and particle sizes has been represented on the basis of systematical characterization of materials aided with computational methods. We believe this study holds promise for significantly shortening the development cycle of electrode materials for lithium ion battery.

[References]

- [1] ZHOU X, WAN L J, GUO Y G. Synthesis of MoS₂ nanosheet-graphene nanosheet hybrid materials for stable lithium storage[J]. Chemical Communications, 2013, 49(18): 1838.

- [2] SATHISH M, TOMAI T, HONMA I. Graphene anchored with Fe_3O_4 nanoparticles as anode for enhanced Li-ion storage[J]. *Journal of Power Sources*, 2012, 217: 85-91.
- [3] CHEN S, WANG Y, AHN H, et al. Microwave hydrothermal synthesis of high performance tin-graphene nanocomposites for lithium ion batteries [J]. *Journal of Power Sources*, 2012, 216: 22-27.
- [4] PARK S K, YU S H, WOO S, et al. A facile and green strategy for the synthesis of MoS_2 nanospheres with excellent Li-ion storage properties [J]. *Cryst Eng Comm*, 2012, 14(24): 8323.
- [5] WINTER M, BRODD R J. What are batteries, fuel cells, and supercapacitors [J]. *Chem Rev* 2004, 104: 4245-4269.
- [6] CHANG K, CHEN W. In situ synthesis of MoS_2 /graphene nanosheet composites with extraordinarily high electrochemical performance for lithium ion batteries [J]. *Chemical Communications*, 2011, 47(14): 4252.
- [7] BRIVIO J, ALEXANDER D T L, KIS A. Ripples and layers in ultrathin MoS_2 embranes [J]. *Nano Letters*, 2011, 11(12): 5148-5153.
- [8] TENNE R, MARGULIS L, GENUIT M, et al. Polyhedral and cylindrical structures of tungsten disulphide [J]. *Letters to Nature*, 1992, 360: 4-6.
- [9] RAMAKRISHNAMATTE H S S, GOMATHI A, MANNA A K, et al. MoS_2 and WS_2 Analogues of graphene [J]. *Angewandte Chemie*, 2010, 122(24): 4153-4156.
- [10] WHITTINGHAM M S, GAMBLE JR F R. The lithium intercalates of the transition metal dichalcogenides [J]. *Materials Research Bulletin*, 1975, 10(5): 363-371.
- [11] WHITTINGHAM M S. The role of ternary phases in cathode reactions [J]. *Journal of The Electrochemical Society*, 1976, 123(3): 315-320.
- [12] DINO T, CHRISTIAN P, JAEGERMANN W. Origin of the electrochemical potential in intercalation electrodes [J]. *J Phys Chem B*, 2004, 108: 6093-6099.
- [13] WANG Q, LI J. Facilitated lithium storage in MoS_2 overlayers supported on coaxial carbon nanotubes [J]. *J Phys Chem C*, 2007, 111: 1675-1682.
- [14] DING S, ZHANG D, CHEN J S, et al. Facile synthesis of hierarchical MoS_2 microspheres composed of few-layered nanosheets and their lithium storage properties [J]. *Nanoscale*, 2012, 4(1): 95.
- [15] KWON J H, AHN H J, JEON M S, et al. The electrochemical properties of Li/TEGDME/ MoS_2 cells using multi-wall carbon nanotubes as a conducting agent [J]. *Research on Chemical Intermediates*, 2010, 36(6/7): 749-759.
- [16] STEPHENSON T, LI Z, OLSEN B, et al. Lithium ion battery applications of molybdenum disulfide (MoS_2) nanocomposites [J]. *Energy & Environmental Science*, 2014, 7(1): 209.
- [17] CATHERINE M. ZELENSKI, DORHOUT P K. Template synthesis of near-monodisperse [J]. *J Am Chem Soc* 1998, 120: 734-742.
- [18] XIANHUI CHEN, FAN R. Low-temperature hydrothermal synthesis of transition [J]. *Chem Mater*, 2001, 13: 802 -805.
- [19] DRESSSELHAUS M S, THOMAS I L. Alternative energy technologies [J]. *Nature*, 2001, 414(6861): 332-337.
- [20] CHANG K, CHEN W X, MA L, et al. Graphene-like MoS_2 /amorphous carbon composites with high capacity and excellent stability as anode materials for lithium ion batteries [J]. *Journal of Materials Chemistry*, 2011, 21(17): 6251.
- [21] YANG L, WANG S, MAO J, et al. Hierarchical MoS_2 /polyaniline nanowires with excellent electrochemical performance for lithium-ion batteries [J]. *Advanced Materials*, 2013, 25(8): 1180-1184.
- [22] MAP Y, HAERING R R. Structural destabilization induced by lithium intercalation in MoS_2 and related compounds [J]. *Canadian Journal of Physics*, 1983, 61: 76-84.
- [23] DU G, GUO Z, WANG S, et al. Superior stability and high capacity of restacked molybdenum disulfide as anode material for lithium ion batteries [J]. *Chemical Communications*, 2010, 46(7): 1106.
- [24] GORDON R A, YANG D, CROZIER E D, et al. Structures of exfoliated single layers of WS_2 , MoS_2 , and MoSe_2 in aqueous suspension [J]. *Physical Review B*, 2002, 65(12): 125407.
- [25] CHEN X, CHEN Z, LI J. Critical electronic structures controlling phase transitions induced by lithium ion intercalation in molybdenum disulphide [J]. *Chinese Science Bulletin*, 2013, 58(14): 1632-1641.
- [26] CHEN X, HE J, SRIVASTAVA D, et al. Electrochemical cycling reversibility of LiMoS_2 using first-principles calculations [J]. *Applied Physics Letters*, 2012, 100(26): 263901.
- [27] JOHN P, KIERON B, ERNZERHOF M. Generalized gradient approximation made simple [J]. *Phys Rev Lett*, 1996, 77: 3865-3868.
- [28] KRESSE G, HAFNER J. Ab initio molecular-dynamics simulation of the liquid-metal-amorphous-semiconductor transition in germanium [J]. *Physical Review B*, 1994, 49(20): 251-269.
- [29] KRESSE G, FURTHMULLER J. Efficient iterative schemes for ab initio total-energy calculations using a plane-wave basis set [J]. *Physical Review B*, 1996, 54(16): 169-186.
- [30] BLOCH P E. Projector augmented-wave method [J]. *Physical Review B*, 1994, 50(24): 953-979.

- [31] GRIMME S. Semiempirical GGA-type density functional constructed with a long-range dispersion correction [J]. *Journal of Computational Chemistry*, 2006, 27(15): 1787-1799.
- [32] CHEN Z, LI J, ZHANG Z. First principles investigation of electronic structure change and energy transfer by redox in inverse spinel cathodes LiNiVO₄ and LiCoVO₄ [J]. *Journal of Materials Chemistry*, 2012, 22(36): 18968.
- [33] NEUGEBAUER J, SCHEFFLER M. Adsorbate-substrate and adsorbate-adsorbate interactions of Na and K adlayers on Al(111) [J]. *Physical Review B*, 1992, 46(24): 16067-16080.
- [34] MAKOV G, PAYNE M. Periodic boundary conditions in ab initio calculations [J]. *Physical Review B*, 1995, 51(7): 4014-4022.
- [35] ZHANG C, WU H B, GUO Z, et al. Facile synthesis of carbon-coated MoS₂ nanorods with enhanced lithium storage properties [J]. *Electrochemistry Communications*, 2012, 20: 7-10.
- [36] HWANG H, KIM H, CHO J. MoS₂ nanoplates consisting of disordered graphene-like layers for high rate lithium battery anode materials [J]. *Nano Letters*, 2011, 11(11): 4826-4830.
- [37] DAS S K, MALLAVAJULA R, JAYAPRAKASH N, et al. Self-assembled MoS₂-carbon nanostructures: influence of nanostructuring and carbon on lithium battery performance [J]. *Journal of Materials Chemistry*, 2012, 22(26): 12988.
- [38] FENG C, MA J, LI H, et al. Synthesis of molybdenum disulfide (MoS₂) for lithium ion battery applications [J]. *Materials Research Bulletin*, 2009, 44(9): 1811-1815.
- [39] FANG X, HUA C, GUO X, et al. Lithium storage in commercial MoS₂ in different potential ranges [J]. *Electrochimica Acta*, 2012, 81: 155-160.
- [40] LIU C, YU Z, NEFF D, et al. Graphene-based supercapacitor with an ultrahigh energy density [J]. *Nano Letters*, 2010, 10(12): 4863-4868.
- [41] GOODENOUGH J B, KIM Y. Challenges for rechargeable li batteries [J]. *Chemistry of Materials*, 2010, 22(3): 587-603.
- [42] CHEN J, TAO Z L, SUO L. Lithium intercalation in open-ended TiS₂ nano-tubes [J]. *Angewandte Chemie*, 2003, 115(19): 2197-2201.
- [43] JULIEN C M. Lithium intercalated compounds charge transfer and related properties [J]. *Materials Science and Engineering R*, 2003, 40: 47-102.
- [44] DAHN J R, ZHENG T, LIU Y, et al. Mechanisms for lithium insertion in carbonaceous materials [J]. *Science*, 1995, 270(5236): 590-593.

(责任编辑 张 晶)